Journal of Alloys and Compounds 509 (2011) 3872–3879

Contents lists available at ScienceDirect

Journal of Alloys and Compounds

journal homepage: www.elsevier.com/locate/jallcom

Fabrication and electrical characterization of 15% yttrium-doped barium zirconate—nitrate freeze drying method combined with vacuum heating

Susumu Imashuku*, Tetsuya Uda, Yoshitaro Nose, Yasuhiro Awakura

Department of Materials Science and Engineering, Kyoto University, Yoshida-Honmachi, Sakyo, Kyoto 606-8501, Japan

ARTICLE INFO

Article history:
Received 6 July 2010
Received in revised form
16 December 2010
Accepted 19 December 2010
Available online 28 December 2010

Keywords:
Barium zirconate
Fuel cell
Grain boundary
Nitrate freeze-drying method

ABSTRACT

We applied a nitrate freeze-drying method to obtain a fine synthesized powder of 15% yttrium-doped barium zirconate. Fine 15% yttrium-doped barium zirconate powder of particle size about 30 nm was obtained by synthesizing at 500 °C in vacuum from a powder mixed by the nitrate freeze-drying method. However, we could not obtain such fine powder by synthesizing in air. Using the powder synthesized in vacuum, large and homogeneous grains of 15% yttrium-doped barium zirconate were easily obtained after sintering. Then, the bulk and grain boundary resistance were evaluated by AC 2-terminal measurement of sample in the form of bar and pellet and DC 4-terminal measurement of bar-shape sample. The grain boundary resistance was not inversely proportional to the grain size as theoretically expected. We concluded that specific grain boundary conductivity varies with samples. Some impurities, evaporation loss of barium oxide and/or other unexpected reasons might affect the grain boundary resistance in 15% yttrium-doped barium zirconate.

1. Introduction

Trivalent cation doped barium zirconates were first reported by Iwahara et al. as proton conductive oxides [1]. At early studies of the doped barium zirconates, reported proton conductivities of the materials were low [1–6]. However, Kreuer reported that single crystal of yttrium-doped barium zirconate had relatively high proton conductivity even at 140 °C (5×10^{-5} S cm^{-1}) [7] and then Bohn and Schober confirmed the high proton conductivity of yttrium-doped barium zirconate at high temperatures (3×10^{-3} S cm^{-1} at 600 °C in wet hydrogen [8]). After their reports, many researchers are working on yttrium-doped barium zirconate and reported the proton conductivity [9–34]. However, the grain boundary resistance of yttrium-doped barium zirconate is higher than the bulk resistance. Thus, it is needed to reduce the grain boundary density. But, as far as we know, it is quite difficult to obtain large grains of 7, 10, and 15% yttrium-doped barium zirconate by sintering at less than 1715 °C with a powder synthesized by solid state reaction method [8,14,21,25,34], although it is relatively easy to obtain well-grown and homogeneous grains of 20% yttrium-doped barium zirconate with a powder synthesized by sintering at even less than 1600 °C [18,23,26,32]. In the case of 15% yttrium-doped barium zirconate ($BaZr_{0.85}Y_{0.15}O_{3-\delta}$), we found that the difficulty was caused by the difference in phase relationship between the sintering temperature (1600 °C) and the synthesizing temperature (1300 °C) [21,25,35]. $BaZr_{0.85}Y_{0.15}O_{3-\delta}$ is in the single phase region at 1600 °C but it is expected to be in a two-phase region of yttrium poor barium zirconate phase and yttrium rich barium zirconate phase at 1300 °C [26,35,36]. Therefore, during sintering, cations have to diffuse mutually over long distance, which might slow the rate of grain growth. Therefore, if the particle size of synthesized powder is finer than that of synthesized powder by the solid state reaction method, it is possible to obtain large and homogeneous grains of yttrium-doped barium zirconate in short time because the diffusion distance for cations becomes shorter during sintering at 1600 °C.

Among various reports for fabrication of finer oxides [37–40], one unique method, called as the nitrate freeze-drying method, was reported for very fine powder of barium titanate ($BaTiO_3$) (10–15 nm) [40]. In this study, we employed the nitrate freeze-drying method, by which there is no report on the synthesis of barium zirconate, to obtain a fine powder of $BaZr_{0.85}Y_{0.15}O_{3-\delta}$ and investigated the sintering behavior and their grain boundary resistances.

2. Experimental

2.1. Material preparation

The reagents used were barium nitrate ($Ba(NO_3)_2$: 99.9%, Wako), zirconyl nitrate dihydrate ($ZrO(NO_3)_2 \cdot 2H_2O$: 97.0%, Wako), and yttrium nitrate *n*-hydrate ($Y(NO_3)_3 \cdot nH_2O$: 99.99%, Wako). The zirconyl nitrate solution contained 2.18 mass% of hafnium (Hf) as an impurity, but the chemical properties of hafnium are quite similar to those of zirconium. Thus, hafnium is expected to occupy the zirconium site and

* Corresponding author. Tel.: +81 75 753 5445; fax: +81 75 753 5284.
E-mail address: materials_process@aqua.mtl.kyoto-u.ac.jp (S. Imashuku).

0925-8388/$ – see front matter © 2010 Elsevier B.V. All rights reserved.
doi:10.1016/j.jallcom.2010.12.140

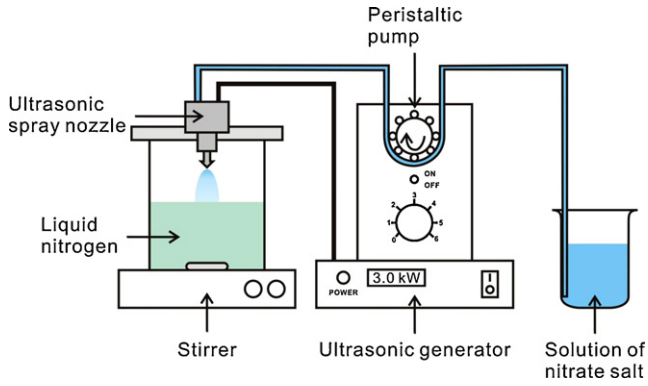

Fig. 1. Schematic view of apparatus for obtaining atomized frozen powder.

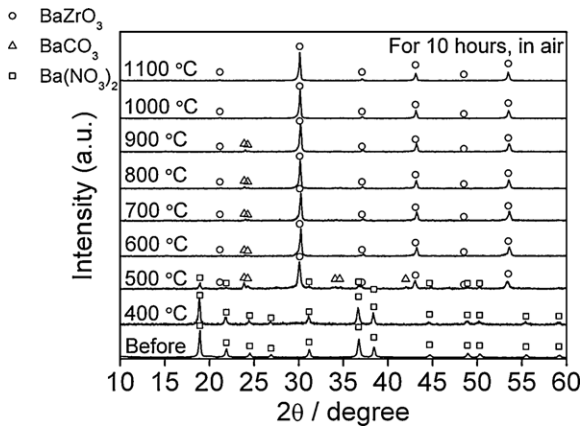

Fig. 2. XRD patterns before and after heating of powder obtained by the nitrate freeze-drying method at 400–1100 °C for 10 h in air.

to behave very much like zirconium. The hydration number of n in yttrium nitrate hydrate was confirmed to be 5.3 by inductive coupled plasma-atomic emission spectroscopy (ICP-AES) (Seiko Instruments Inc., SPS4000). Zirconyl nitrate dihydrate was dissolved in 0.1 M nitric acid and the solution was filtered by Teflon paper filter of pore size 0.2 μm to remove a small amount of zirconia (ZrO_2) in the solution. Yttrium nitrate hydrate was dissolved in 0.1 M nitric acid (HNO_3). The concentrations of the two solutions were measured by ICP-AES, and the solutions and barium nitrate powder were mixed to produce Ba:(Zr + Hf):Y = 1:0.85:0.15. The concentration of barium, zirconium, and yttrium ions in the mixed solution was measured again by ICP-AES in order to confirm that the molar ratio of the metal ions in the mixed solution was what we desire (Ba:Zr + Hf:Y = 1:0.85:0.15). Then, the mixed solution was atomized using an ultrasonic spray nozzle (Sonotek, 06-5108) and rapidly frozen by leading the aerosol to fall into stirred liquid nitrogen as shown in Fig. 1. The frozen solution was vacuum-dried in a freeze dryer (DRC-1100 and FDU-2100, EYEA) operated at reduced pressure and temperature (5 Pa, −40 °C), while monitoring the temperatures of the frozen solution using a thermocouple. The temperature in the frozen solution indicated a constant value (about −43 °C) until the sublimation of the solution finished. We determined the end of sublimation by checking the rise in temperature of the frozen solution. The temperature of the freeze dryer was quite gradually increased to 25 °C. When the powder was completely dried at 25 °C, the vacuum chamber was backfilled with air and the resulting freeze-dried powder was stored in a sealed bottle. The freeze-dried powder was heated at various temperatures (400–1100 °C) in air or vacuum (~10^{-5} atm) in order to determine the condition where only barium zirconate phase was obtained. The powder was then ball-milled for 10 h and the powder was pressed into a pellet, whose diameter and thickness were about 10 mm and 1.5 mm, respectively, or a bar, whose height, width and thickness were about 5, 35 and 1 mm, respectively, at 392 MPa. Subsequently, the pellet was sintered at 1600 °C in a sacrifice powder (90 mass% of synthesized barium zirconate and 10 mass% of $BaCO_3$) to avoid BaO loss due to the high vapor pressure of BaO at high temperature. The pellets or bars of sacrifice powder were placed on an alumina boat and sintered in a pure oxygen atmosphere.

2.2. Material characterization

Microstructures of the synthesized powders and sintered pellets were observed by a scanning electron microscope (SEM, Keyence Corporation, VE-7800) and transmission electron microscope (TEM) (JEOL, JEM-2010). Compositional analysis was carried out using energy dispersive X-ray microanalysis (EDX) (JEOL, JED-2300) with a field emission-scanning electron microscope (FE-SEM) (JEOL, JSM-6500F) and ICP-AES. The densities of the sintered pellets were measured by the Archimedes method using ionic liquid (trimethyl-n-hexylammonium bis((trifluoromethyl)sulfonyl) amide (TMHA-Tf_2N)). The lattice parameters of the sintered pellets were determined by XRD analysis of Cu-Kα (XRD, PANalytical, X'Pert-ProMPD) and the theoretical density was estimated by the lattice parameters.

2.3. Conductivity measurement

Conductivity was measured by the DC 4-terminal method and the AC 2-terminal method. The sintered bar was used for the DC 4-terminal measurement. Platinum wire was wound around the bar, and silver paste (Fujikura Kasei) was painted around the interface between the platinum wire and electrolyte as electrodes. The data were collected using a potentiogalvanostat (Solartron SI 1287).

The sintered pellet and bar were used for the AC 2-terminal measurement. When the pellet was used for the measurement, silver paste was painted on both surfaces of the pellet as electrodes after mechanically polishing the surface of the pellet. Electrodes for the bar were prepared in the same way for the DC 4-terminal measurement with a minor difference of employing only two 2 terminals in this case. The data were collected using a frequency response analyzer (Solartron SI 1260) in a frequency range of 10 Hz to 7 MHz with applied voltages of 100 mV. An equivalent circuit model was fitted to the data by Zplot (Scribner Associates Inc., NC).

The data of the DC 4-terminal method and the AC 2-terminal method were collected in argon (Ar) gas with water vapor pressure of 5.2×10^{-2} atm. Before the start of each experiment, the bar and pellet were held at 700 °C for at least 18 h for hydration, and kept at 600 °C for at least 5 h until the impedance spectrum remained constant for more than 5 h. Conductivity was measured at 80 and 600 °C. In the cases where measurements were carried out at 80 °C, the conductivity was measured after equilibration at 600 °C with water vapor pressure of 5.2×10^{-2} atm and cooled to 80 °C at a rate of 0.2 °C min^{-1}.

3. Results and discussion

3.1. Synthesis conditions

Fig. 2 shows XRD patterns of synthesized powder heated at 400–1100 °C for 10 h in air. No peak was detected from zirconia on powder before heating because freeze-dried zirconyl nitrate was amorphous. At temperatures above 500 °C, barium zirconate phase was detected, but a small amount of barium carbonate or barium nitrate was identified. At temperatures above 1000 °C, complete reaction was confirmed. However, the particle size of the yttrium-doped barium zirconate was larger than that obtained by the solid state reaction method synthesized at 1300 °C for 10 h in air and ball-milled for 100 h as shown in Fig. 3. The reason for the large particle size might be related to the formation of liquid phase of barium nitrate (melting point: 592 °C).

To prevent barium nitrate from melting, the powder mixed by the nitrate freeze-drying method was heated in a vacuum (~10^{-5} atm) in order to accelerate the decomposing reaction of barium nitrate to barium oxide (BaO). Fig. 4 shows XRD patterns of powders obtained by the nitrate freeze-drying method and synthesizing at 400–600 °C for 10 h in a vacuum. At temperatures higher than 500 °C, only the barium zirconate phase was identified and the particle size of the yttrium-doped barium zirconate powder obtained by the nitrate freeze-drying method and synthesizing at 500 °C for 10 h in vacuum was much finer than that at 1000 °C in air as shown in Fig. 3. The particle size was found to be about 30 nm as shown in the photograph of TEM in Fig. 5(a).

The particle size of the yttrium-doped barium zirconate powder obtained by the solid state reaction method at 1300 °C for 10 h in air followed by ball-milling for 100 h was about 40 nm as shown in the photograph of TEM in Fig. 5(b). Thus, the slightly finer particle of the yttrium-doped barium zirconate powder could be obtained by the nitrate freeze-drying method and synthesis at 500 °C for 10 h in a vacuum.

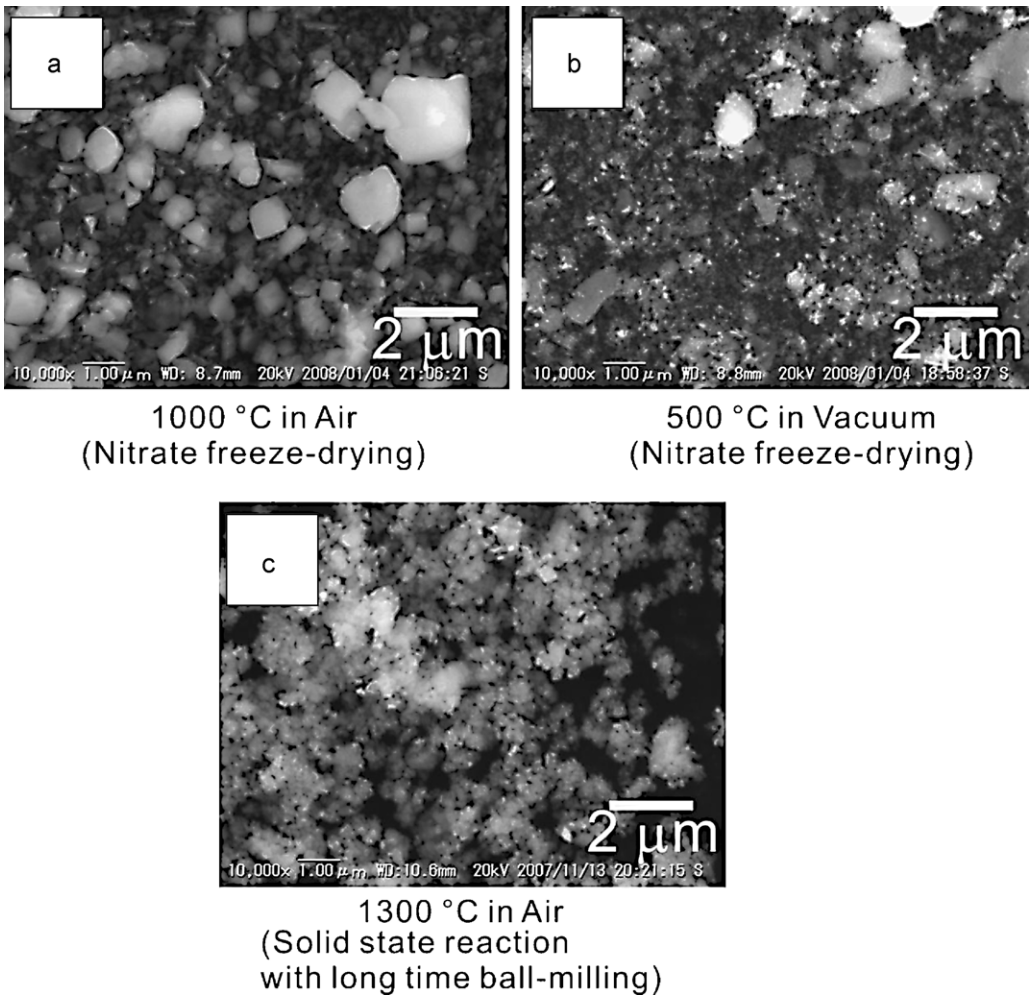

Fig. 3. SEM image of yttrium-doped barium zirconate powders obtained by the nitrate freeze-drying method and synthesis (a) at 1000 °C for 10 h in air and (b) at 500 °C for 10 h in vacuum with (c) yttrium-doped barium zirconate powder obtained by solid state reaction method at 1300 °C for 10 h in air and ball-milling for 100 h.

3.2. Sintering behavior

Fig. 6 shows cross-sectional SEM images and results of composition analysis by EDX of $BaZr_{0.85}Y_{0.15}O_{3-\delta}$ bars sintered for 4, 24 and 100 h using powders synthesized at 500 °C for 10 h in vacuum, and the average grain size is summarized in Table 1. We obtained large and homogeneous grains in a shorter time by the nitrate freeze-drying method. In comparison, when we used powders by solid state reaction method at 1300 °C, a sintering time of 100 h was required to obtain large and homogeneous grains as shown in Fig. 6. Thus, the sintering behavior between the nitrate freeze drying method and the solid state reaction method was quite different. However, there is not a big difference of particle sizes between the powders synthesized by the two different methods. We consider that there is a phase separation of yttrium-doped barium zirconate in the powder synthesized by the solid state reaction method because a phase separation of quite small amount of yttrium doped barium zirconate and a new phase called BZ(II) [36] phase was reported at lower temperature than 1600 °C [35]. On the other hand, we assume that there is no phase separation in the powder synthesized at 500 °C in vacuum from the powder mixed by the nitrate freeze-drying method, because the synthesis at low temperatures suppresses the phase separation kinetically.

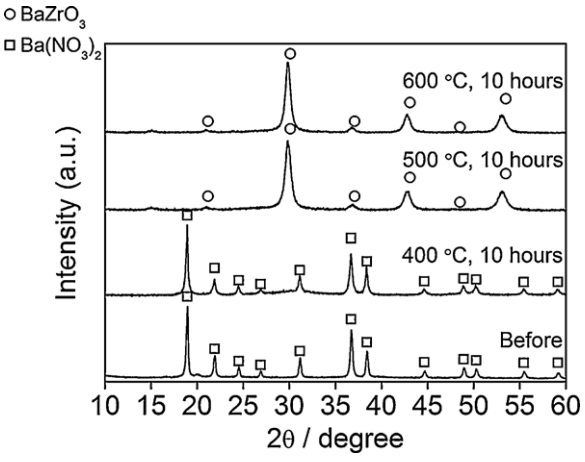

Fig. 4. XRD patterns of powders obtained by the nitrate freeze-drying method and synthesis at 400–600 °C for 10 h in vacuum.

3.3. Conductivity measurement

3.3.1. Interpretation of impedance spectra

Fig. 7 shows AC 2-terminal impedance spectrum of $BaZr_{0.85}Y_{0.15}O_{3-\delta}$ bars sintered for 24 h from powders synthesized

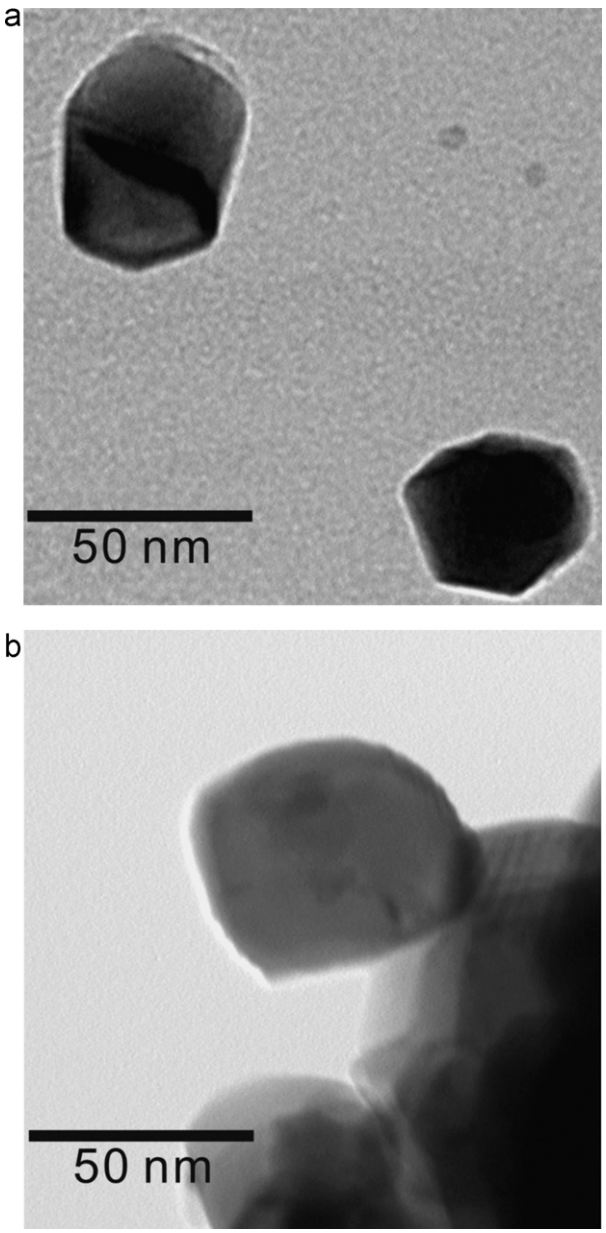

Fig. 5. TEM image of $BaZr_{0.85}Y_{0.15}O_{3-\delta}$ powders (a) obtained by the nitrate freeze-drying method and synthesis at 500 °C for 10 h in vacuum and (b) obtained by solid state reaction method at 1300 °C for 10 h in air and ball-milling for 100 h.

by the nitrate freeze-drying method at 600 °C in wet argon, and three arcs (Arc 1, Arc 2 and Arc 3) were observed. In order to determine the arcs due to the electrolyte, resistivity of the $BaZr_{0.85}Y_{0.15}O_{3-\delta}$ was measured by DC 4-terminal method in wet argon. The time-dependant change of voltage between the two inner terminals was measured by the DC 4-terminal measurement in the $BaZr_{0.85}Y_{0.15}O_{3-\delta}$ with applied DC current of 10 μA in wet argon as shown in Fig. 8. The voltage increased with time, which might be affected by polarization at the outer electrodes. Thus, the voltage before the start of polarization was evaluated for electrolyte resistivity calculation. The current–voltage characteristics of the $BaZr_{0.85}Y_{0.15}O_{3-\delta}$ at 600 °C in wet argon are shown in Fig. 9. From the figure, the resistivity of the $BaZr_{0.85}Y_{0.15}O_{3-\delta}$ at 600 °C in wet argon was determined to be 65.0 Ω cm. Compared to Fig. 7, 65.0 Ω cm corresponds to the value of the right edge of Arc 3. Therefore, we can say that Arc 1 and Arc 2 come from electrodes and that Arc 3 comes from the electrolyte.

According to the past report [7], another arc due to bulk should exist at a higher frequency region of Arc 3, but it was not clear even at low temperature as seen in Fig. 10(a). The reason for the unclear arc is considered to be that the capacitance of the arc at the left side of Arc 3 was too small (less than 10^{-13} F) to determine the resistance and capacitance accurately with the frequency response analyzer we used. Therefore, we changed L/S of sample to increase the capacitance by the use of sample which has a shape of pellet. Fig. 10(b) shows the impedance spectrum of the $BaZr_{0.85}Y_{0.15}O_{3-\delta}$ in the pellet form at 80 °C in wet argon. In the figure, a new arc (Arc 4) was observed clearly at the left side of Arc 3 and the capacitance of Arc 4 was 5.9×10^{-11} F. The dielectric constant of Arc 4 was calculated from

$$C = \frac{S}{L}\varepsilon\varepsilon_0 \quad (1)$$

where L is the sample length, S is the sample cross sectional area, ε is dielectric constant, and ε_0 is dielectric constant of vacuum. The calculated dielectric constant of Arc 4 was 60. This value agrees with the dielectric constant of bulk reported by Kreuer using single crystal [7]. Thus, this result also supports that Arc 4 comes from bulk.

However, it was difficult to obtain the value of grain boundary resistance (Arc 3) at 600 °C in wet argon using a pellet as shown in Fig. 11. Thus, determination of the grain boundary resistance at higher temperatures requires the conductivity measurement in bar form or the change of electrode material.

3.3.2. Dependence of grain size on conductivity

Impedance spectra of $BaZr_{0.85}Y_{0.15}O_{3-\delta}$ for various sintering times and synthesizing methods were measured at 80 °C for pellets and 600 °C for bars in wet argon, and the results are shown in Fig. 12(a) and (b), respectively. The arc at the highest frequency region at 80 °C corresponds to bulk and that at 600 °C is due to grain boundary, and the bulk conductivities and inverse of grain boundary resistances at 80 °C and total conductivities at 600 °C are summarized in Table 1. From Fig. 12(a), there is not a large difference in bulk resistances. As for grain boundary resistance of the bar sintered from powder of the nitrate freeze-drying method combing with heating at 500 °C for 10 h in vacuum, the grain boundary resistance decreased by changing the sintering time from 4 h to 24 h as shown in Fig. 12(b). This might be because of the increase of grain size from 0.52 μm in the bar sintered for 4 h to 0.92 μm for 24 h. However, the grain boundary resistance of the bar sintered for 100 h increased though larger grains (1.06 μm) were obtained, which implies that factors other than grain boundary affects the grain boundary resistance. On the other hand, as shown in Table 1, the grain boundary resistance at 80 °C had different trend from that at 600 °C. This might be because it is difficult to separate the arc due to grain boundary low temperature such as 80 °C owing to the overlap with the arcs due to grain boundary and electrode at low frequency region.

The inverse of grain boundary resistance, $1/R_{g.b.}$, depends on specific grain boundary conductivity, $\sigma^{\circ}_{g.b.}$, and effective grain boundary thickness, g, in addition to grain size, G, as shown in [41]

$$\frac{L}{S}\frac{1}{R_{g.b.}} = \frac{C_{bulk}}{C_{g.b.}}\sigma^{\circ}_{g.b.} = \frac{G}{g}\sigma^{\circ}_{g.b.} \quad (2)$$

where C_{bulk} and $C_{g.b.}$ are capacitances of bulk and grain boundary, respectively. The value, $C_{bulk}/C_{g.b.}$, which are evaluated from

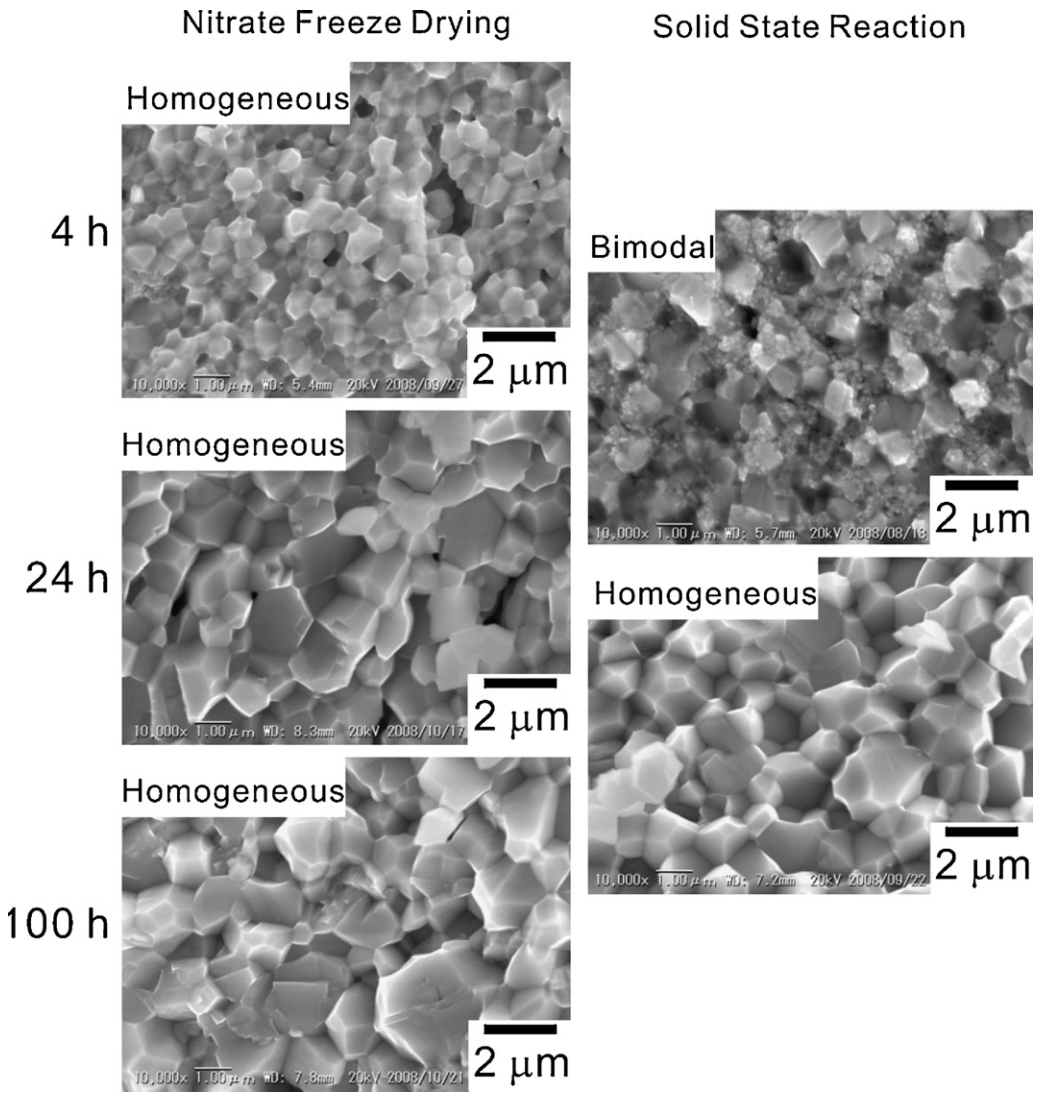

Fig. 6. Cross-sectional SEM image of $BaZr_{0.85}Y_{0.15}O_{3-\delta}$ bars sintered for 4, 24 and 100 h at 1600 °C from powders obtained by using the nitrate freeze-drying method and synthesis at 500 °C for 10 h in vacuum and by solid state reaction method at 1300 °C for 10 h in air.

impedance spectra at 80 °C, and effective grain boundary thicknesses are calculated from grain sizes. These values are listed in Table 1. The effective grain boundary thicknesses were the same order as reported values [17,31,41] and almost constant for any synthesis and sintering conditions in this study. This suggests that the specific grain boundary conductivity changed with samples. We hypothesized two reasons of reduction of specific grain boundary conductivity as follows:

(1) Impurity phases precipitated at grain-boundaries. Sodium and silicon were confirmed by qualitative analysis by ICP-AES.
(2) Barium oxide preferentially vaporized at grain-boundaries during sintering because barium oxide has a significantly high vapor pressure at the sintering temperature, 1600 °C.

The reason (2) might be related to the report that barium loss in 20% yttrium-doped barium zirconate and gadolinium-doped barium cerate leads to the decrease of the bulk and total conductivity, respectively [18,42]. Actually, yttria phase was additionally identified in the samples sintered for 100 h from both powders of the nitrate freeze-drying and solid state reaction method by XRD. The precipitation of yttria phase is due to the barium loss in the samples as we reported previously [21]. Also, we made a barium deficient sample ($Ba_{0.95}Zr_{0.85}Y_{0.15}O_{3-\delta}$) and confirmed the increase of grain boundary resistance as seen in Fig. 13. In Fig. 13, both pellets are sintered for 24 h using powder synthesized at 500 °C for 10 h in vacuum from the powder mixed by the nitrate freeze-drying method.

We also investigated the reproducibility of grain boundary resistances in the bar sintered for 24 h from powders synthesized by the nitrate freeze-drying method. Three individual batches of $BaZr_{0.85}Y_{0.15}O_{3-\delta}$ (batch—1, 2 and 3) powder were synthesized by the nitrate freeze-drying method, and sintered for 24 h. Fig. 12(c) shows the impedance spectra at 600 °C in wet argon and there is great variability in the grain boundary resistance among batches. Considering this result, we think that both factors and other unexpected reason might contribute to the unclear behavior of specific grain boundary conductivity.

Table 1
Relative density, grain size, total conductivity at 600 °C, bulk conductivity at 80 °C, inverse of grain boundary resistance at 80 °C, the ratio of electric capacity of bulk to grain boundary, and effective grain boundary thickness of $BaZr_{0.85}Y_{0.15}O_{3-\delta}$.

Synthesizing method	Sintering hour (h)	Relative density (%)	Grain size (μm)	σ_{bulk} at 80 °C[a] ($S\,cm^{-1}$)	$\frac{l}{S}\frac{1}{R_{g.b.}}$ at 80 °C[a] ($S\,cm^{-1}$)	σ_{total} at 600 °C[b] ($S\,cm^{-1}$)	$C_{bulk}/C_{g.b.}$	Effective grain boundary thickness[c] (nm)
Nitrate freeze-drying	4	85.0	0.51	2.1×10^{-5}	1.3×10^{-7}	9.8×10^{-3}	2.4×10^{-2}	12
Nitrate freeze-drying	24	97.4	0.92	2.2×10^{-5}	2.9×10^{-7}	1.5×10^{-2}	1.3×10^{-2}	12
Nitrate freeze-drying	100	99.0	1.06	2.6×10^{-5}	6.5×10^{-7}	9.3×10^{-3}	1.1×10^{-2}	12
Solid state reaction	100	100	1.00	2.2×10^{-5}	4.8×10^{-7}	1.1×10^{-2}	1.3×10^{-2}	13

[a] The values are obtained in the form of the pellet.
[b] The values are obtained in the form of the bar.
[c] Grain boundary thickness is calculated from Eq. (2).

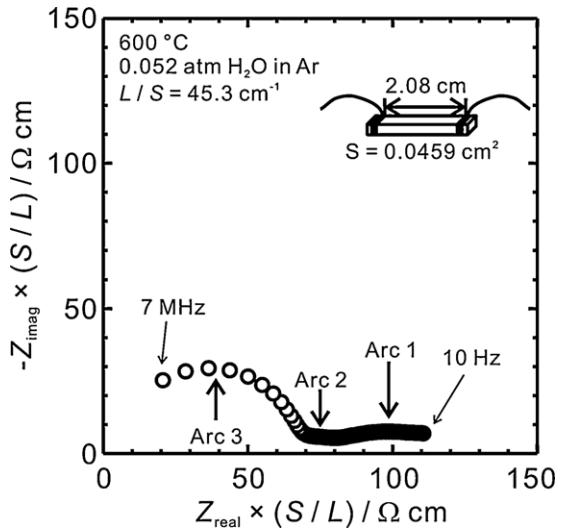

Fig. 7. AC 2-terminal impedance spectrum at 600 °C in Ar–5.2% H_2O using a bar of $BaZr_{0.85}Y_{0.15}O_{3-\delta}$ sintered for 24 h from powders obtained by using the nitrate freeze-drying method and synthesis at 500 °C for 10 h in vacuum.

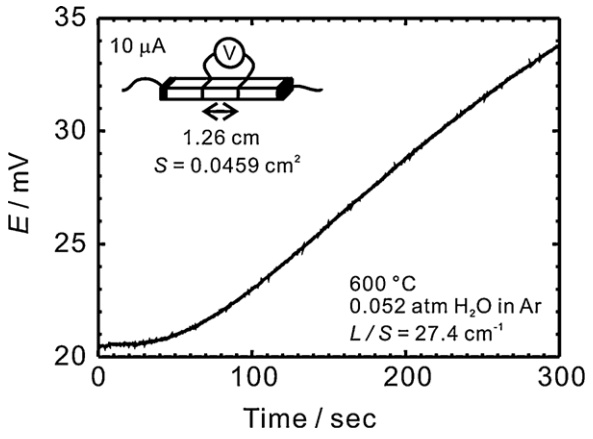

Fig. 8. Time-dependant change of voltage between two inner terminals of $BaZr_{0.85}Y_{0.15}O_{3-\delta}$ bars sintered for 24 h from powders obtained by using the nitrate freeze-drying method and synthesis at 500 °C for 10 h in vacuum. DC current of 10 μA was applied in the DC 4-terminal measurement at 600 °C in Ar–5.2% H_2O.

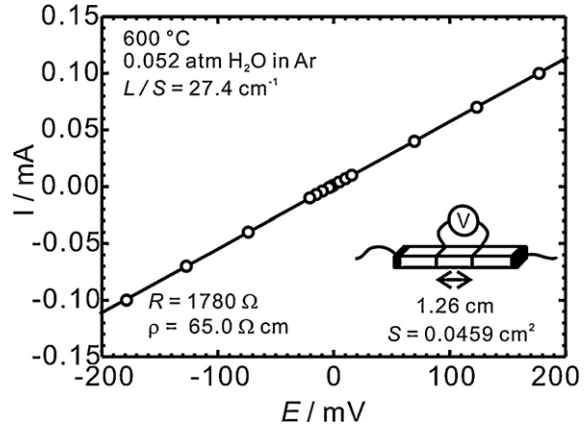

Fig. 9. Current–voltage characteristic of $BaZr_{0.85}Y_{0.15}O_{3-\delta}$ bars sintered for 24 h from powders obtained by using the nitrate freeze-drying method and synthesis at 500 °C for 10 h in vacuum in the DC 4-terminal measurement at 600 °C in Ar–5.2% H_2O.

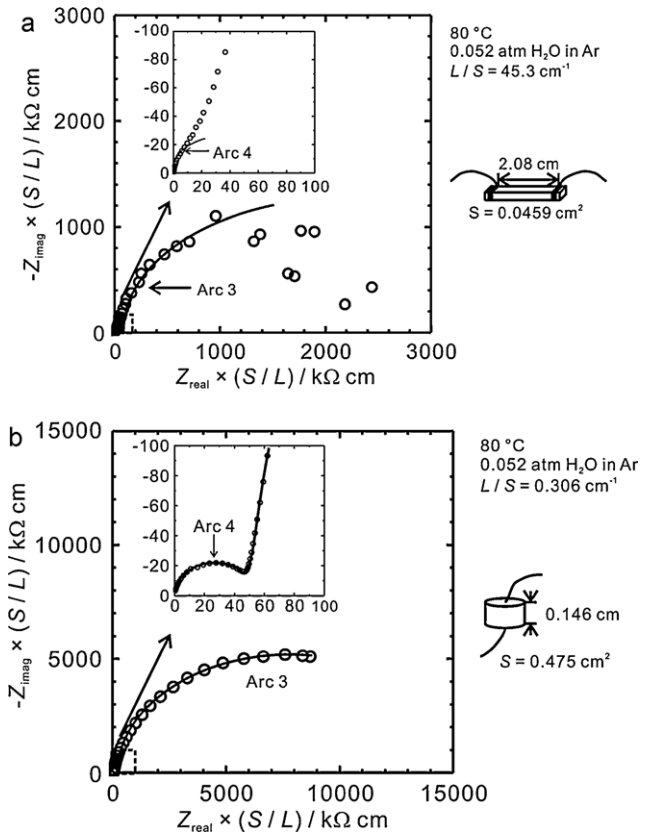

Fig. 10. Effect of different shape of samples on AC 2-terminal impedance spectrum in Ar–5.2% H_2O (a) using a bar of $BaZr_{0.85}Y_{0.15}O_{3-\delta}$ and (b) using a pellet of $BaZr_{0.85}Y_{0.15}O_{3-\delta}$ at 80 °C. $BaZr_{0.85}Y_{0.15}O_{3-\delta}$ was sintered for 24 h from powders obtained by using the nitrate freeze-drying method and synthesis at 500 °C for 10 h.

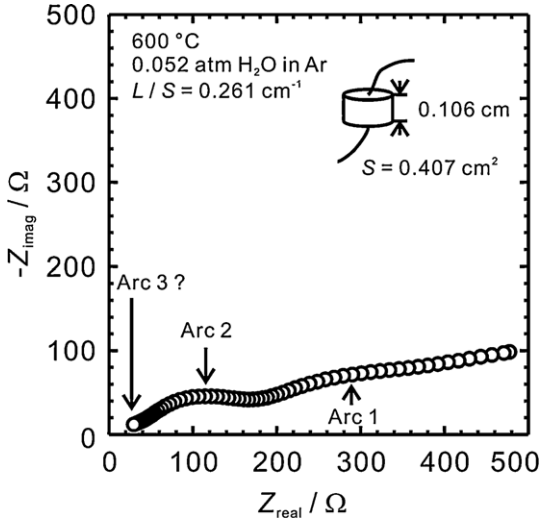

Fig. 11. AC 2-terminal impedance spectrum at 600 °C in Ar–5.2% H_2O using a pellet of $BaZr_{0.85}Y_{0.15}O_{3-\delta}$ sintered for 24 h from powders obtained by using the nitrate freeze-drying method and synthesis at 500 °C for 10 h.

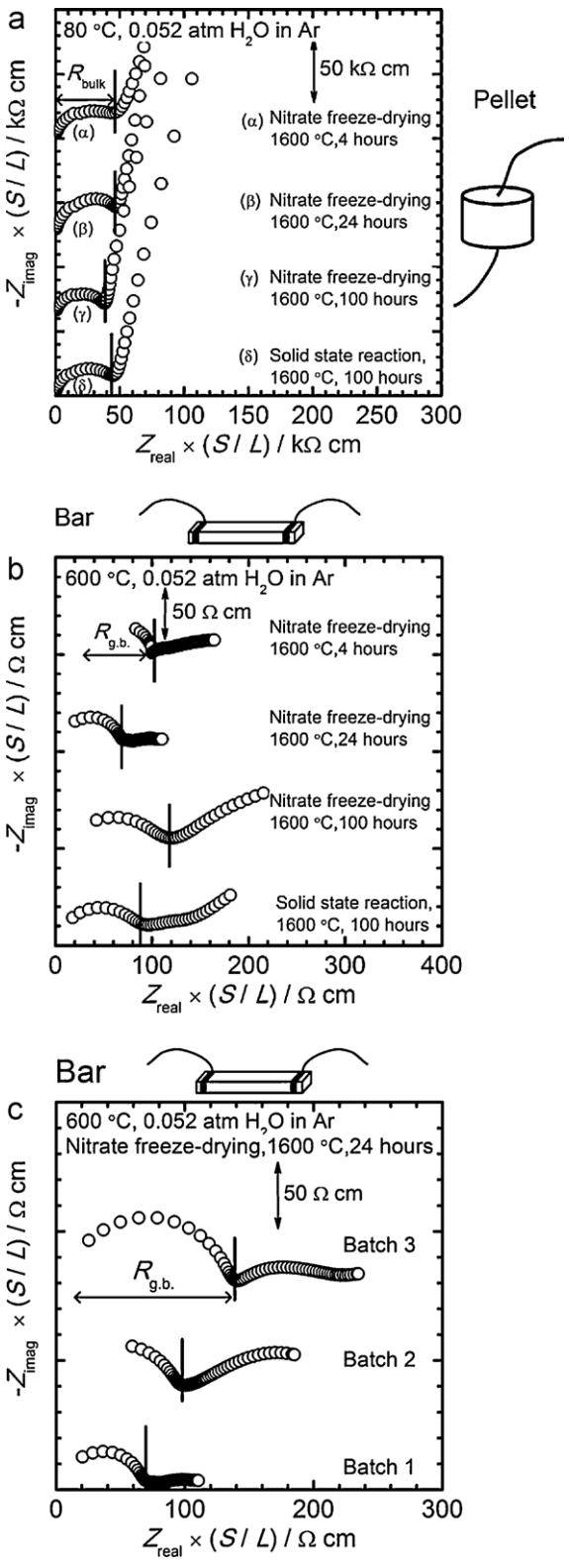

Fig. 12. AC 2-terminal impedance spectra in Ar–5.2% H_2O of $BaZr_{0.85}Y_{0.15}O_{3-\delta}$ at (a) 80 °C using pellets, (b) 600 °C using bars and (c) comparison of AC 2-terminal impedance spectra of three batches of $BaZr_{0.85}Y_{0.15}O_{3-\delta}$ sintered for 24 h at 1600 °C from powders obtained by using the nitrate freeze-drying method and synthesis at 500 °C for 10 h. The sintering time and synthesis method are indicated in the figure.

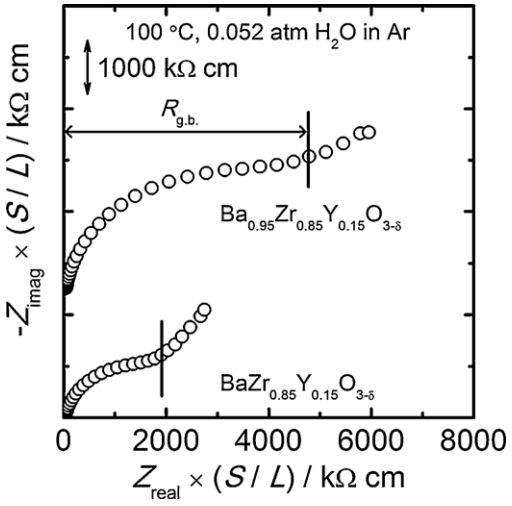

Fig. 13. AC 2-terminal impedance spectra in Ar–5.2% H_2O of $Ba_{0.95}Zr_{0.85}Y_{0.15}O_{3-\delta}$ and $BaZr_{0.85}Y_{0.15}O_{3-\delta}$ pellets sintered for 24 h from powder synthesized at 500 °C for 10 h in vacuum from the powder mixed by the nitrate freeze-drying method at 100 °C.

4. Conclusions

The results obtained in this work can be summarized as follows:

(1) Fine 15% yttrium-doped barium zirconate powder was obtained by synthesizing at 500 °C in vacuum from powder mixed by the nitrate freeze-drying method. Vacuum heating was essential to obtain fine powder.
(2) Large and homogeneous grains of 15% yttrium-doped barium zirconate are obtained using such fine powders and short sintering time.
(3) Grain boundary resistance of the 15% yttrium-doped barium zirconate was not improved although larger grains were obtained. Specific grain boundary conductivity might vary with samples. Also, the reproducibility using different batches of powder was poor in the measurement of grain boundary resistance.

Acknowledgements

This study was supported by the Industrial Technology Research Grant Program in 2006 from New Energy and Industrial Technology Development Organization (NEDO) of Japan. A part of this study was also financially supported by Grant-in-Aid for JSPS Fellows (00202005). We express our deep acknowledgement to Mr. K. Kazumi for TEM images. Also, we are grateful to Mr. T. Tanaka for his assistance of conductivity measurement.

References

[1] H. Iwahara, T. Tajima, T. Hibino, K. Ozaki, H. Suzuki, Solid State Ionics 61 (1993) 65–69.
[2] A. Manthiram, J.F. Kuo, J.B. Goodenough, Solid State Ionics 62 (1993) 225–234.
[3] R.C.T. Slade, S.D. Flint, N. Singh, Solid State Ionics 82 (1995) 135–141.
[4] S. Wienstrijer, H.D. Wiemhijfer, Solid State Ionics 101–103 (1997) 1113–1117.
[5] K.H. Ryu, S.M. Haile, Solid State Ionics 125 (1999) 355–367.
[6] V.P. Gorelov, V.B. Balakireva, Y.N. Kleschchev, V.P. Brusentsov, Inorg. Mater. 37 (2001) 535–538.
[7] K.D. Kreuer, Solid State Ionics 125 (1999) 285–302.
[8] H.G. Bohn, T. Schober, J. Am. Ceram. Soc. 83 (2000) 768–772.
[9] T. Schober, H.G. Bohn, Solid State Ionics 127 (2000) 351–360.
[10] K. Katahira, Y. Kohchi, T. Shimura, H. Iwahara, Solid State Ionics 138 (2000) 91–98.
[11] K.D. Kreuer, S. Adams, W. Munch, A. Fuchs, U. Klock, J. Maier, Solid State Ionics 145 (2001) 295–306.
[12] M. Laidoudi, I. Abu Talib, R. Omar, J. Phys. D: Appl. Phys. 35 (2002) 397–401.
[13] F.M.M. Snijkers, A. Buekenhoudt, J. Cooymans, J.J. Luyten, Scr. Mater. 50 (2004) 655–659.
[14] W.S. Wang, A.V. Virkar, J. Power Sources 142 (2005) 1–9.
[15] C.D. Savaniu, J. Canales-Vazquez, J.T.S. Irvine, J. Mater. Chem. 15 (2005) 598–604.
[16] K. Nomura, H. Kageyama, Solid State Ionics 178 (2007) 661–665.
[17] F. Iguchi, N. Sata, T. Tsurui, H. Yugami, Solid State Ionics 178 (2007) 691–695.
[18] P. Babilo, T. Uda, S.M. Haile, J. Mater. Res. 22 (2007) 1322–1330.
[19] S.B.C. Duval, P. Holtappels, U.F. Vogt, E. Pomjakushina, K. Conder, U. Stimming, T. Graule, Solid State Ionics 178 (2007) 1437–1441.
[20] S.W. Tao, J.T.S. Irvine, J. Solid State Chem. 180 (2007) 3493–3503.
[21] S. Imashuku, T. Uda, Y. Awakura, Electrochem. Solid State Lett. 10 (2007) B175–B178.
[22] A.K. Azad, C. Savaniu, S. Tao, S. Duval, P. Holtappels, R.M. Ibberson, J.T.S. Irvine, J. Mater. Chem. 18 (2008) 3414–3418.
[23] A. D'Epifani, E. Fabbri, E. Di Bartolomeo, S. Licoccia, E. Traversa, Fuel Cells 8 (2008) 69–76.
[24] S. Higgins, N.M. Sammes, A. Smirnova, J.A. Kilner, G. Tompsett, J. Fuel Cell Sci. Technol. 5 (2008) 011003.
[25] S. Imashuku, T. Uda, Y. Nose, K. Kishida, S. Harada, H. Inui, Y. Awakura, J. Electrochem. Soc. 155 (2008) B581–B586.
[26] R.B. Cervera, Y. Oyama, S. Miyoshi, K. Kobayashi, T. Yagi, S. Yamaguchi, Solid State Ionics 179 (2008) 236–242.
[27] J.H. Shim, T.M. Gür, F.B. Prinz, Appl. Phys. Lett. 92 (2008) 253115.
[28] P.A. Stuarta, T. Unnob, J.A. Kilnera, S.J. Skinner, Solid State Ionics 179 (2008) 1120–1124.
[29] S. Imashuku, T. Uda, Y. Nose, G. Taniguchi, Y. Ito, Y. Awakura, J. Electrochem. Soc. 156 (2009) B1–B8.
[30] Z. Khani, M. Taillades-Jacquin, G. Taillades, M. Marrony, D.J. Jones, J. Rozière, J. Solid State Chem. 182 (2009) 790–798.
[31] F. Iguchi, T. Tsurui, N. Sata, Y. Nagao, H. Yugami, Solid State Ionics 180 (2009) 563–568.
[32] Y. Yamazaki, R. Hernandez-Sanchez, S.M. Haile, Chem. Mater. 21 (2009) 2755–2762.
[33] S.B.C. Duval, P. Holtappels, U.F. Vogt, U. Stimming, T. Graule, Fuel Cells 5 (2009) 613–621.
[34] S. Imashuku, T. Uda, Y. Nose, Y. Ito, Y. Awakura, J. Alloy. Compd. 409 (2010) 672–676.
[35] S. Imashuku, T. Uda, Y. Nose, Y. Awakura, J. Phase. Equilib. Diff. 31 (2010) 348.
[36] Y. Oyama, X. Li, S. Miyoshi, S. Yamaguchi, 14th International Conference on Solid State Protonic Conductors, Kyoto, 2008, p. 120.
[37] B. Grob, C. Beck, F. Meyer, T. Krajewski, R. Hempelmann, H. Altgeld, Solid State Ionics 145 (2001) 325–331.
[38] I. Antunes, A. Brandão, F.M. Figueiredo, J.R. Frade, J. Grácio, D.P. Fagg, J. Solid State Chem. 182 (2009) 2149–2156.
[39] M.M. Bucko, J. Obłakowski, J. Eur. Ceram. Soc. 27 (2007) 3625–3628.
[40] J.M. McHale, P.C. McIntyre, K.E. Sickafus, N.V. Coppa, J. Mater. Res. 11 (1996) 1199–1209.
[41] S.M. Haile, D.L. West, J. Campbell, J. Mater. Res. 13 (1998) 1576–1595.
[42] D. Shima, S.M. Haile, Solid State Ionics 97 (1997) 443–455.